ELSEVIER

Synthetic Metals 87 (1997) 211–217

SYNTHETIC METALS

Physical properties of CVD-grown Se–carbon films

L. Grigorian [a], S. Fang [a], G. Sumanasekera [a], A.M. Rao [a], L. Schrader [b], P.C. Eklund [a,*]

[a] *Department of Physics and Astronomy and Center for Applied Energy Research, University of Kentucky, Lexington, KY 40506, USA*

[b] *University of the South, Sewanee, TN 37383, USA*

Received 29 October 1996; accepted 20 December 1996

Abstract

A novel chemical vapor deposition (CVD) approach based on the thermal decomposition of an aromatic hydrocarbon in the presence of Se vapor is used to grow films of layered Se–carbon compounds. In principle, this technique can produce a wide variety of new carbon-based materials, for example, graphite intercalation compounds (GICs) which, for kinetic reasons, cannot be made if the intercalant vapor has to diffuse large distances into a pre-existing graphitic host. In particular, homogeneous oriented submicron films of either pure stage-3 ($Se_{24}C$) or mixed-stage Se–carbon layer compounds have been successfully grown on Ni substrates in evacuated sealed quartz tubes. X-ray diffraction, X-ray photoelectron spectroscopy, Raman scattering and the *c*-axis electrical transport measurements are discussed in terms of both covalent Se–carbon bonding and an ionic model assuming the formation of an acceptor-type Se–GIC with electron transfer from carbon to Se. Our CVD-grown Se–carbon films exhibit the largest thermoelectric power reported in the open literature among carbon-based compounds. However, the value is at least a factor of 10 less than reported for these materials in patents by Sharp Corp.

Keywords: Graphite–Se; Graphite intercalation compounds; Electrical transport; Chemical vapor deposition; Films; X-ray diffraction; Raman scattering

1. Introduction

Traditionally, graphite intercalation compounds (GICs) are produced by exposing a pre-existing graphitic host, such as highly oriented pyrolytic graphite (HOPG), to the vapor or solution of the intercalant species (such as alkali, alkaline and rare-earth metals, halogens, halides, etc.) which then must diffuse at least several microns into the host graphite [1,2]. This kinetic limitation makes it impractical to apply traditional intercalation techniques to insert a number of potentially interesting intercalants, e.g., Se, Te, Ge, Si, etc.

A new, chemical vapor deposition (CVD) approach to produce GICs has been recently reported in patents by the Sharp Corp. in Japan [3,4]. Their approach used a flowing mixture of a hydrocarbon (such as benzene) which supplies carbon atoms for growth of the graphitic host, and a vapor containing the guest species such as an organometallic reagent, metal halide or elemental metal. An inert carrier gas (argon) was used to transport the vapors of reagents to the hot zone of the furnace where the hydrocarbon molecules undergo decomposition due to the combined effect of high temperature and catalytic action of a transition metal (e.g., Ni) substrate. The guest species were captured between growing graphitic carbon layers, and the resultant materials were reported to form a series of new GICs [3,4]. In their method, both the formation of the graphitic host and the intercalation occur at the same time, so that the diffusion kinetics is no longer a limiting factor. The CVD-grown graphite and GIC films were reported to be highly oriented, with the *c*-axis of the microcrystals aligned normal to the substrate. Some of these materials were found by the Sharp Corp. Group to exhibit unusually high *c*-axis thermoelectric power, $S = 150$–$900\ \mu V/K$ [3]. Moreover, they found that the samples also demonstrated very high values of the thermoelectric figure of merit:

$$Z = S^2\sigma/\kappa \qquad (1)$$

where σ and κ are, respectively, the *c*-axis electrical and thermal conductivities. In the particular cases of Se–GICs and Te–GICs, experimental values of $ZT > 30$ were reported [3], that is more than an order of magnitude larger than that of any previously known thermoelectric material. If this result can be verified, these materials would represent a major breakthrough in the field of thermoelectrics.

However, very little structural and spectroscopic data were reported for the Sharp Corp. samples, and the physical origin of the anomalous thermoelectric properties was not investigated. To the best of our knowledge, no other group has reproduced the synthetic route or the remarkably high ther-

* Corresponding author. Fax: +1 606 257 6725.

PII S0379-6779(97)03809-5

moelectric figure of merit. In this work, we present the results on synthesis and characterization of homogeneous oriented submicron films of Se–carbon layered compounds grown by a closed-tube CVD method. Open-tube CVD experiments in the Se–carbon system are underway in our group, and the results will be reported later. Results of X-ray diffraction (XRD), X-ray photoelectron spectroscopy (XPS), Raman scattering, *c*-axis electrical resistivity and thermoelectric power measurements on these films are reported and discussed.

It is important to note that in our closed-tube CVD system, the reactor volume is gradually being filled with hydrogen released with the decomposition of the hydrocarbon precursor. The presence of hydrogen in the closed-tube system may affect the reaction in several possible ways, e.g., through reaction with Se vapor to form H_2Se, H-termination of dangling carbon bonds in the growing graphite film, affecting the film growth process and the composition and structure of the resulting layer compound. This aspect makes our CVD approach different from the open-tube CVD process used by the Sharp Corp. Group where all the gaseous by-products of the reaction and unreacted precursors are removed from the film growth zone by the argon carrier gas stream.

2. Synthesis and experimental details

A schematic arrangement of reactants and the substrate in our closed-tube approach is shown in Fig. 1. The method can be generalized to a wide variety of volatile reagents and is ideal for toxic precursors such as Se, since all the reagents and reaction products are contained within the reaction tube. The Ni substrates were first cleaned from oxide and other surface contamination by a few seconds immersion in a mixture of 150 ml of sulfuric and 225 ml of nitric acids and 100 ml of water, followed by rinsing with de-ionized water and methanol. As a hydrocarbon source, we used anthracene or naphthalene, since they are solids at room temperature and their vapor pressure is easily controlled by the sublimation rate at moderate temperatures near 100–400 °C. We have found that the reaction product was the same, independent of whether anthracene or naphthalene was used as the carbon precursor. Therefore, anthracene was chosen mainly on the basis of handling convenience.

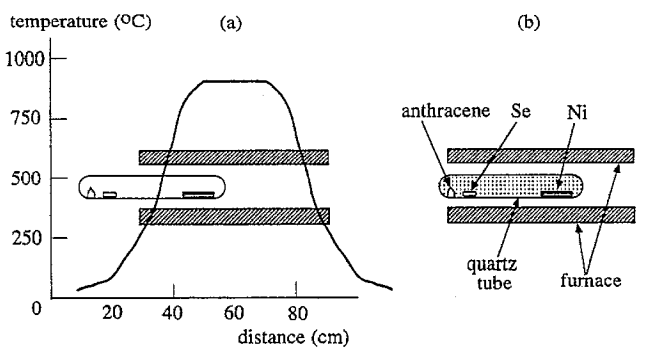

Fig. 1. Schematic of the closed-tube CVD experiment for growing Se–carbon films. Position of the reaction tube is shown during (a) the pre-growth and the annealing stages, and (b) the film growth process.

The anthracene powder and Se shots were loaded in one end of a 50 cm long quartz tube, the Ni substrate in the other end, and the tube was sealed under a vacuum of 10^{-3} Torr. The Ni-containing end was introduced into a pre-heated furnace to allow the Ni substrate to warm up first, while the reagents were kept at room temperature (Fig. 1(a)). After the Ni substrate's temperature reached 900 °C, the tube was pushed further into the furnace to a pre-determined position so that the anthracene and Se were maintained at temperatures of about 350 and 500 °C, respectively (Fig. 1(b)). In a short time, both hydrocarbon and Se start subliming, their vapors spread over the tube reaching the hot zone, and the Se–carbon film starts growing on the Ni substrate as the anthracene decomposes. To terminate the growth process and anneal the film, the reagent-containing end of the tube was pulled out of the furnace while the sample-containing end was kept at 900 °C (Fig. 1(a)). The annealing procedure usually took 10 to 20 h and was designed to condense all the unreacted hydrocarbon, Se and possible reaction by-products at the cold end of the tube, as well as improve the quality of the Se–carbon films. After annealing, the furnace was switched off and the tube was allowed to cool to room temperature over 2–3 h. As a measure of safety when handling Se and possibly its volatile derivatives such as H_2Se (which is very toxic), the tube was opened carefully in a chemical hood, and the film samples were extracted from the tube without direct contact using a permanent magnet. Similar to the observation made by the Sharp Corp. Group [3], we have also found that the films were stable in laboratory air. The chemical composition and quality of the grown films could be controlled through control of the temperatures of the reagents and that of the Ni substrate, as well as the molar ratio of Se to carbon in the precursors.

We have found it very important to synchronize the initiation of the sublimation processes to ensure that both the reagents reach the Ni substrate simultaneously. If either the Se or the hydrocarbon vapor reached the Ni substrate first, the Ni substrate would be covered either with nickel selenide (which readily forms at these conditions) or pyrolytic graphite. In either case, the Se–carbon layer compound films were found to contain impurity phases. In addition, the parts of the Ni substrate covered with nickel selenide become catalytically ineffective, thereby disrupting the growth of Se–carbon film. However, by manipulating the temperature at the Se and hydrocarbon source, predominantly single-phase Se–carbon films could be grown. Adhesion of the CVD-grown films to the Ni substrates varied from sample to sample, and was observed to be much better if the film deposition rate was equal or lower than 0.1 μm/h. Typical film thickness values were about 0.5 μm. As expected, better adhesion correlated with careful cleaning of the Ni substrate.

XRD patterns of the CVD-grown films were taken using a Rigaku X-ray diffractometer (Cu Kα radiation). Raman scattering spectra were measured with an Ar laser (514.5 nm

radiation) in the Brewster-angle back-scattering configuration using a single grating, f/5, 0.46 m monochromator (Jobin–Yvon HR460) equipped with a 'supernotch' filter (Kaiser Optical) and a charge-coupled array detector. The X-ray photoemission measurements were carried out using an LHS-11 XPS spectrometer (Mg Kα radiation). D.c. electrical resistivity was measured in the direction perpendicular to the surface (i.e. parallel to the *c*-axis) using the four-probe geometry described below. The electrical contacts to the films were made with silver paint (DuPont). Thickness of the films was determined by observing the film cross section with a scanning electron microscope (Hitachi). Thermoelectric power measurements were carried out with an experimental set-up described elsewhere [5], in which two identical copper–constantan thermocouples electrically contacting the sample are used to determine simultaneously the temperature difference and Seebeck voltage in the direction parallel to the *c*-axis.

3. Results

3.1. XRD

Without Se present in the reaction tube, high-quality graphitic films were obtained at $T_{Ni} = 900$ °C, where T_{Ni} is temperature of the Ni substrate, as evidenced by sharp reflections observed in the XRD pattern (Fig. 2(a)). The scattering vector was oriented perpendicular to the film surface, and this geometry was also used for the Se–carbon films. Comparison with the X-ray pattern of a commercial highly oriented pyrolytic graphite (HOPG) prepared by Union Carbide shows that our film exhibits even sharper reflections (a typical full width at half-maximum (FWHM) in our films is 0.19° versus 0.28° in HOPG). Strongly enhanced (00*L*) reflections from the film grown at $T_{Ni} = 900$ °C indicate that the film is preferentially oriented with the graphitic *c*-axis perpendicular to the substrate. The presence of a weak (101) peak indicates that some of the crystallites are not perfectly aligned, i.e., their basal plane was tipped out of the plane of the substrate. The X-ray data also show that the film has an A–B–A–B-type graphitic crystal structure with the interplanar separation of 3.365 Å, which is only slightly higher than the separation of 3.354 Å observed in the HOPG sample, and significantly less than the value of 3.40 Å observed for turbostratic graphite [1].

When Se vapor was also present in the reaction tube, the XRD patterns changed completely due to the incorporation of Se layers into the crystal structure of the graphitic host (Fig. 2(b)). Usually, the Se-containing samples exhibited XRD patterns which could be interpreted as arising from a mixture of various stage Se–carbon layered compounds with $n = 2$–5, as inferred from the values of the *c*-axis repeat distance (I_c) calculated from the experimentally observed (00*L*) reflections. The stage index *n* refers to the number of carbon layers present between successive intercalate layers

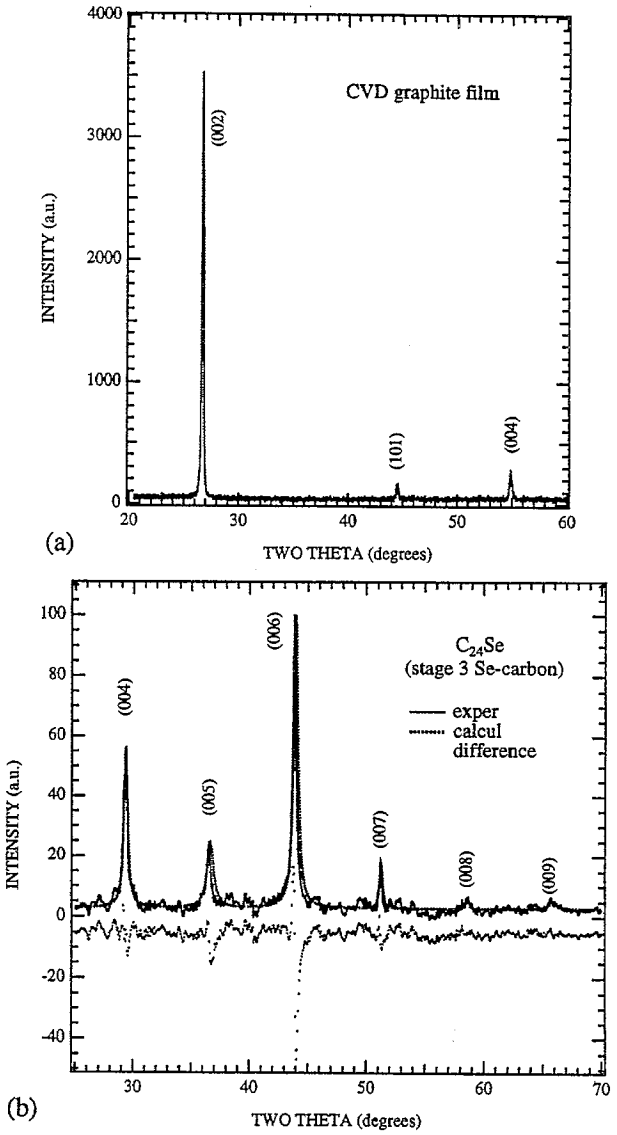

Fig. 2. XRD patterns of the CVD-grown films of (a) graphitic carbon, oriented with its *c*-axis perpendicular to the surface, and (b) stage-3 Se–carbon (the difference curve is shifted for clarity).

[1]. In addition to the relatively sharp reflections (FWHM ~ 0.5°) identified with various stage Se–carbon phases, many of the samples exhibited a broad (FWHM = 1 to 10–15°) background at diffraction angle $2\theta \sim 25°$ coming from poorly crystallized graphitic carbon.

We were able to grow a few films of a Se–carbon layered compound which exhibited only the reflections expected for a pure stage-3 compound (Fig. 2(b)). The (00*L*) XRD intensities for these stage-3 Se–carbon film samples were analyzed within the framework of the model developed by Boca et al. [6] for $SbCl_5$–GICs according to

$$I_{00L}(\text{calc}) = KLPA|F_{00L}|^2 \quad (2)$$

where $I_{00L}(\text{calc})$ are the calculated XRD intensities of the (00*L*) reflections, F_{00L} is the structure factor, *K* is a scale factor, and *L*, *P* and *A* are the angle-dependent Lorentz, polar-

ization and absorption factors, respectively. The structure factor is calculated according to

$$F_{00L} = \sum N_j f_j \exp(2\pi i z_j L) \exp(-B_j \lambda^{-2} \sin^2\theta_L) \quad (3)$$

where N_j is the atomic density in the jth atomic layer, f_j is the atomic scattering factor, z_j is the layer coordinate and B_j is the Debye–Waller factor. The XRD intensities calculated using the Eqs. (2) and (3) were compared to the experimental data using a least-squares fit procedure until an optimal set of parameters was found.

The least-squares fit to the experimental XRD data yielded the following parameters: $I_c = 12.18$ Å (stage 3), corresponding to a carbon–carbon interlayer spacing of 3.40 Å, a Se layer thickness of 1.98 Å and the concentration ratio of Se:C = 1:24. The resulting layer coordinates are summarized in Fig. 3(a). The carbon and Se layers were presumed to be planar, and the thickness of a Se layer obtained from the best fit is very close to the size of a Se^{2-} ion (1.98 Å), and significantly larger than the size of a neutral Se atom (1.17 Å).

Alternative structural models assuming covalent bonding between Se and carbon can also be discussed. Covalent C–Se–C bonding might be anticipated given the very small difference in electronegativity between Se and carbon. Two possible ways to bond Se atoms to graphitic carbon layers are shown in Fig. 3(b)–(c). The first way is to have Se covalently bonded to two carbon atoms within the same layer (pendant model, Fig. 3(b)), similar to what has been suggested for 'graphite oxide' [7]. This type of Se–C bonding could be realized due to reaction of Se with aromatic fragments while in the vapor phase, and then the benzene rings with the attached Se 'pendants' would condense onto Ni substrate into a pendant-model film. Since Se is bonded only to one of the adjacent bounding carbon layers, the Se layer would presumably be expected to be displaced from the central position between the bounding carbon layers. The second way is to have bridging linkages with carbon atoms in adjacent layers (bridging model, Fig. 3(c)). The bridging, as well as the ionic, geometries are not likely to be formed in the vapor phase, but have to be formed during the film growth process. In both the bridging and the ionic models, the Se atoms (ions) are forced to be in the center between the bounding carbon layers. In other words, the layer coordinate of Se is $z_1 = \pm\alpha$ for the pendant model, and $z_1 = 0$ for the bridging and the ionic Se^{2-} models. The value of α depends on the choice of the specific carbon atoms to which the Se bonds and the induced puckering in the carbon layer. Finally, having both $+\alpha$ and $-\alpha$ values reflects the fact that statistically both 'down'-bonded and 'up'-bonded Se are equally possible.

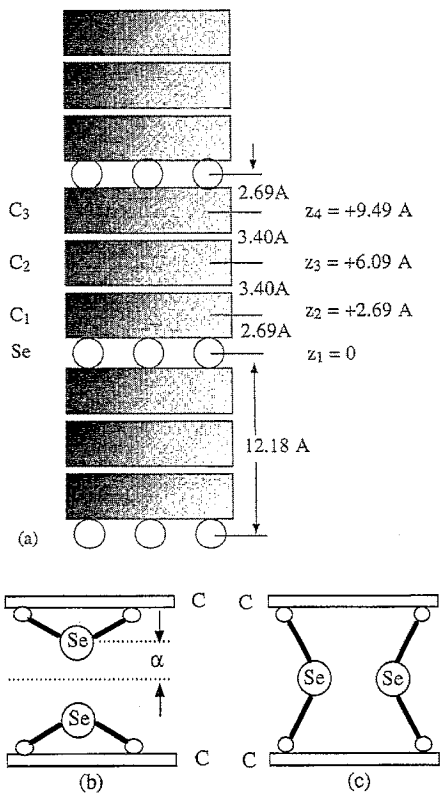

Fig. 3. (a) Ionic structural model for Se–carbon layer materials stacked along the effective c-axis used for the calculation of XRD patterns. (b) Pendant schematic model and (c) bridging schematic model for covalent Se–C bonds. The carbon atoms (small circles) bonded to Se atoms (large circles) are depicted as protruding out of the graphitic carbon layer (rectangles) to show local distortion.

It should be noted that if the Se is covalently attached to the carbon layers, then strictly speaking, the resulting compounds should not be called GICs, but rather Se–carbon layer compounds, as ionic bonding and charge transfer between intercalate and carbon layers in GICs are generally required. Furthermore, and consistent with this view of a GIC, electrical transport in the GIC is modeled as if all the carbon atoms have an sp^2 hybrid configuration, and no significant distortions occur in the in-plane, hexagonal arrangement of the carbon atoms. If the Se has, in fact, covalently attached to the bounding carbon layers, then one would expect a considerable local distortion in the in-plane C–C bonding, as the participating carbon atoms would have an sp^3 rather than an sp^2 configuration, and corresponding changes in the electronic structure must occur. Under these conditions, a host–guest relationship is not an appropriate description of the physical system.

Our structural analysis of the (00L) XRD data show that, as the value of α is increased beyond 0.15 Å, the χ^2 values describing the misfit between theory and experiment diverge sharply. Although the number of reflections analyzed is small (6), this result suggests that a central or near-central position is most likely for the Se, suggesting the pendant model is not favored. However, it is not entirely clear if an $\alpha \cong 0.15$ displacement is large enough to support the pendant model. This would depend on the extent of attendant puckering in the carbon layers. Further discussion on this point will have to wait for higher quality films exhibiting more (00L) reflections.

3.2. XPS

XPS spectra of a stage-3 Se–carbon film (Fig. 4) were measured in the regions of 295–280 (C(1s)) and 60–50 eV (Se(3d)). A single asymmetric peak with effective FWHM ~ 2 eV was observed at a binding energy of 284.3 eV, very close to that of a pure graphite. An up- or down-shift of the C(1s) peak relative to the 284.3 eV peak, as well as a change in linewidth, has been reported in donor- and acceptor-type GICs, respectively, apparently due to charge transfer between the intercalant and graphite (see the review of Schogl in [2]). However, in the cases of high intercalation stages ($n > 2$), the charge-transfer-induced shift is usually below 0.5 eV, that is, much smaller than the experimental linewidth (about 2 eV). Apparently, it is very difficult to expect a small charge-transfer shift to be visible in the case of our broad asymmetric C(1s) peak. On the other hand, the weak asymmetric peak at around 56 eV (FWHM ~ 3 eV) can be assigned to covalently bound Se, similar to that found in organometallic compounds such as $(BrC_6H_4)_2Se_2$ [8]. However, we cannot rule out the possibility of Se^{2-} (ionic model) on the basis of the XPS data, as we could not find any XPS spectra for Se^{2-} reference compounds. Also, no XPS peaks due to nickel selenide at binding energies of 55–54 eV were detected.

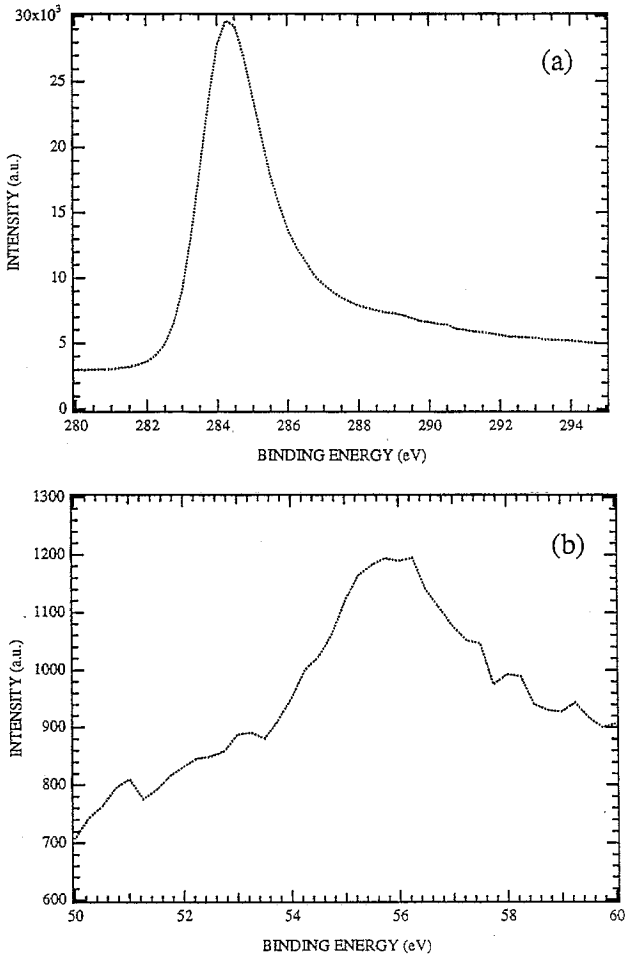

Fig. 4. High-resolution core-level XPS spectra of the stage-3 Se–carbon film taken with a gold reference: (a) C(1s) and (b) Se(3d).

3.3. Raman scattering spectra

The same films used for the XRD measurements were also studied by Raman scattering. We measured Raman spectra at several different spots on each film and found that all the spectra were identical, indicating that the films were homogeneous over the surface area on a length scale of 1 mm (the height of the illuminated streak on the sample). Also, we have compared the Raman spectra of the Se–carbon film taken before the reaction tube was opened, to that taken after the Se–carbon film was removed and exposed to air. No detectable difference was noticed, leading to the conclusion that the samples are stable under ambient conditions at least over several days.

The non-intercalated CVD graphite film exhibited Raman spectra characterized by a weak broad band at 1353 cm^{-1} (Fig. 5(a)). This band is due to disorder-induced first-order scattering and its intensity has been correlated with the finite basal plane crystallite size in the carbon layers [1]. A sharp, stronger peak at 1582 cm^{-1} is identified with the Raman-allowed E_{2g} mode (Fig. 5(a)). Using the ratio of integrated

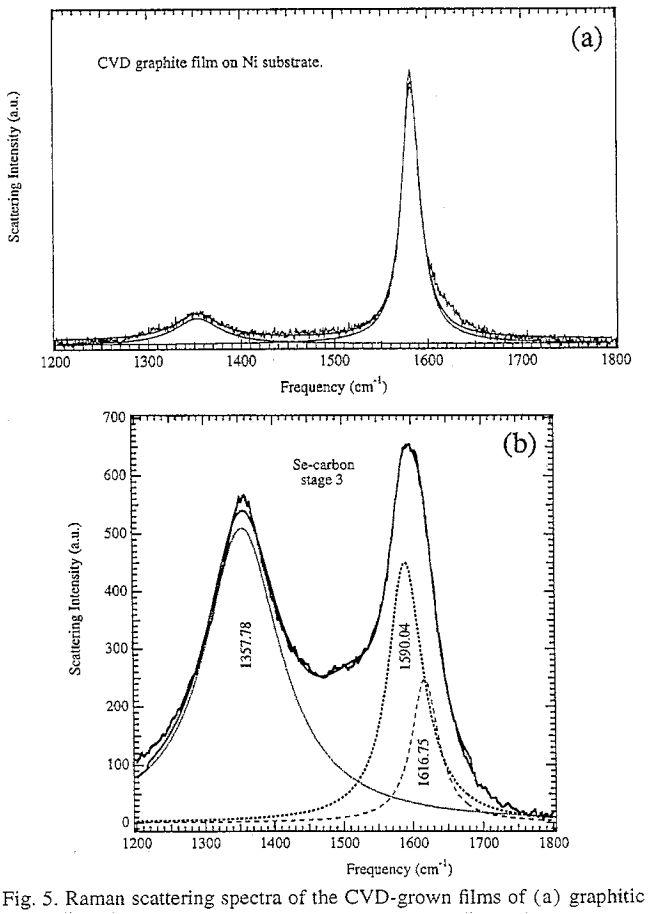

Fig. 5. Raman scattering spectra of the CVD-grown films of (a) graphitic carbon and (b) stage-3 Se–carbon.

intensities of the 1353 and 1582 cm^{-1} bands we have estimated the basal-plane crystallite size to be about 180 Å which is comparable to the value of 200 Å obtained in Ref. [9] for CVD-grown graphite. The Se–carbon films exhibit two broad major features in the Raman spectrum: an intense band at 1358 cm^{-1} and a poorly resolved doublet with peaks at 1590 and 1617 cm^{-1} (Fig. 5(b)). The significant intensity of the 1358 cm^{-1} band indicates a dramatic (at least an order of magnitude) decrease in basal crystallite size and possibly structural disorder in the hexagonal sp^2 carbon network. Part of the intensity of the 1358 cm^{-1} band can probably be ascribed to an amorphous carbon impurity phase also present in the films. This phase would be difficult to detect by XRD due to broadening of reflections.

According to past research in traditional GICs [1,2], the high-frequency E_{2g} intralayer mode of the host graphite is split into a doublet. The lowest frequency peak in this doublet is close in frequency to that of graphite (1582 cm^{-1}) and is identified with carbon layers not adjacent to intercalate layers (i.e., interior carbon layers). The higher frequency component is usually up-shifted in acceptor compounds and is identified with carbon layers which lie next to intercalate layers (i.e., bounding carbon layers) and therefore receive most of the transferred holes from the intercalate layer.

Two peaks are observed in our stage-3 Se–carbon film, one at 1590 and the other at 1617 cm^{-1}. They are identified with E_{2g} modes in the interior (1590 cm^{-1}) and the bounding (1617 cm^{-1}) carbon layers. Consistent with the previous acceptor-type GIC results, the Raman bands in the Se–carbon film were up-shifted with regard to the high-frequency E_{2g} mode of the pure graphite film observed at 1582 cm^{-1}. We can conclude that these high-frequency bands in our Se–carbon films, although considerably broader than those observed in HOPG-based acceptor GICs, are consistent with the formation of an acceptor-type GIC, that is, a GIC, where electron transfer from C to the guest layers has occurred. This result agrees with the sign of the Seebeck coefficient as discussed below.

For GICs, the values of the frequency shift for both the interior and bounding carbon layer modes were found to be roughly proportional to the inverse stage number, $1/n$ [1]. The shift was always found to be positive (up-shift) for the acceptor-type GICs, and negative (down-shift) for the donor-type ones. The interior and the bounding layer frequencies we have obtained for the stage-3 Se–carbon film, that is 1590 and 1617 cm^{-1}, match reasonably well with the typical values observed for other acceptor-type stage-3 GICs [1].

3.4. Transport measurements

Electrical resistivity measurements were carried out as a function of temperature using d.c. current density of about 0.1 mA/mm^2 for the stage-3 and the mixed-stage (2+3) Se–carbon films along the *c*-axis and the data are shown in Fig. 6. The d.c. resistivity of the Se–carbon films was found to be about two orders of magnitude higher as compared to the

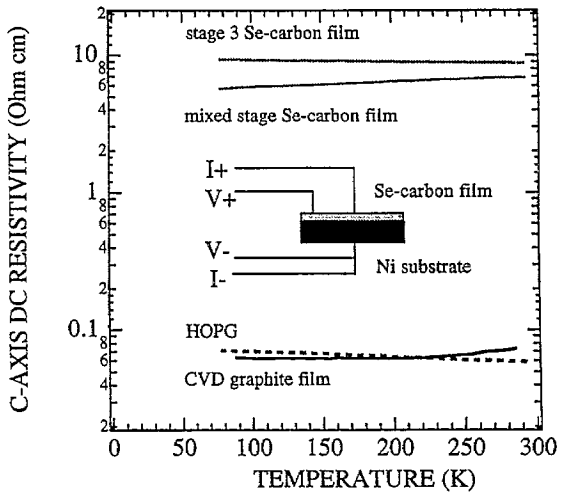

Fig. 6. The *c*-axis electrical resistivity vs. temperature for the HOPG slab and the CVD-grown graphitic carbon film, as well as stage-3 and mixed-stage (2+3) Se–carbon films. The inset shows the geometry of electrical contacts.

non-intercalated reference samples (CVD-grown graphitic film and HOPG) and exhibited very weak dependence on temperature within the range of 77 to 300 K. The temperature coefficient of resistivity was negative for the stage-3 film and positive for the mixed-stage sample. Typically, the in-plane resistivity decreases significantly upon intercalation with both donors and acceptors [10,11]. However, the change in the *c*-axis resistivity has been shown to be sensitive to the type of intercalant: it decreases dramatically for donor-type GICs, but increases for acceptor-type GICs, and the increase was found be as high as several orders of magnitude, depending on the particular intercalant and the stage index [10,11]. For example, the room-temperature *c*-axis resistivity values of 1.1 and 4.2 $\Omega\ cm^{-1}$ observed for the AsF_5-GIC [10] and H_2SO_4–GIC [11] samples are quite close to our results presented in Fig. 6. Thus, the preliminary electrical resistivity data for our Se–carbon films are also in a good agreement with traditional acceptor-type GIC behavior.

An alternative explanation for the observed decrease of conductivity upon Se incorporation can be identified with the puckering of the carbon layers induced by the C–Se–C covalent bond, leading to local distortions of the in-plane conjugation. A similar situation has been found in the case of graphite oxide, where oxygen atoms are believed to be covalently bound to carbon atoms in a fashion similar to our pendant model (Fig. 3(b)), resulting in puckered graphite layers and insulating behavior [7]. In our case, the damage to the *c*-axis conductivity should be less severe, as the concentration of Se in our samples is quite low: the carbon-to-intercalant ratio is 24:1 for Se versus 0.5:1 for oxygen in the graphite oxide.

We have carried out preliminary measurements of a *c*-axis thermopower in several Se–carbon films at 290 K in order to determine the sign of charge carriers and test the potential of these samples as thermoelectric materials, following the claim of giant thermopower and *ZT* values [3]. All the meas-

ured films exhibited positive Seebeck coefficient indicating a p-type conductivity consistent with the assumption of an acceptor-type GIC. The largest c-axis Seebeck coefficient value observed in our Se–carbon films so far was 45 μV/K, higher than any previous in-plane or c-axis value in any GICs or other carbon-based material [1,2,12], but still much lower than that claimed by the Sharp Corp. Group (i.e., 900 μV/K [3]). The other key factor in the thermoelectric figure of merit Z (Eq. (1)) is the ratio of electrical to thermal conductivities, σ/κ, and this ratio may be improved significantly with Se intercalation in spite of the observed decrease in σ. Indeed, for non-magnetic solids, the total thermal conductivity, κ_{total} is contributed mainly by an electronic term (κ_e) and a lattice term (κ_l): $\kappa_{total} = \kappa_e + \kappa_l$ [12]. The electronic term is directly proportional to electrical conductivity according to the Wiedemann–Franz law [12], and the decrease in σ may be compensated with a corresponding decrease in κ_e. On the other hand, the introduction of high atomic mass Se layers into the graphitic crystal structure, as well as structural defects due to intercalation, is expected to suppress the sound velocity (or Debye temperature). Stacking faults may also provide an important phonon scattering mechanism, and both these effects should lead to a decreased lattice term κ_l resulting in an overall improvement of the σ/κ ratio and therefore in Z.

4. Conclusions

We have shown that homogeneous oriented submicron films of Se–carbon layered compounds can be grown by the CVD method in sealed quartz tubes. Our experimental data on XRD and XPS, as well as Raman scattering and the c-axis electrical transport measurements can be reasonably explained with either the covalent Se–carbon bonding models, or the ionic model assuming the formation of an acceptor-type Se–GIC with electron transfer from carbon to Se. The weight of the experimental evidence indicates that a GIC classification for these Se–carbon layer compounds is probably correct, although further work on better quality films will be necessary to clarify the ionic versus covalent nature of the Se–C bonding. The CVD-grown Se–carbon films exhibit the largest thermoelectric power observed so far among the carbon-based compounds.

Acknowledgements

The authors would like to thank G. Dresselhaus, M.S. Dresselhaus and G. Mahan for useful comments. This work was funded in part by grants from ARPA, No. MDA 972-95-1-0021 (G.S., S.F., P.C.E. and A.M.R.), and NSF EPSCOR, No. OSR 9452895 (L.G. and L.S.).

References

[1] M.S. Dresselhaus and G. Dresselhaus, *Adv. Phys., 30* (1981) 139.
[2] S.A. Solin and H. Zabel (eds.), *Graphite Intercalation Compounds*, Vols. I and II, Springer, Berlin, 1990 and 1992.
[3] H. Nakaya, Y. Yoshimoto, M. Yoshida and S. Nakajima, *Eur. Patent Application No. 92 301 388.2* (1992).
[4] Y. Yoshimoto, S. Tomonari, Y. Higashigaki, S. Nakajima and K. Inoguchi, *US Patent No. 5 273 778* (1993).
[5] P.C. Eklund and A.K. Mabatah, *Rev. Sci. Instrum., 48* (1977) 775.
[6] M.H. Boca, M.L. Saylors, D.S. Smith and P.C. Eklund, *Synth. Met., 6* (1983) 39.
[7] G.R. Hennig, Interstitial compounds of graphite, in F.A. Cotton (ed.), *Progress in Inorganic Chemistry*, Vol. 1, Interscience, New York, 1959.
[8] G. Malmsen, I. Thoren, S. Hogberg, J.E. Bergmark and S.E. Karlsson, *Phys. Scr., 3* (1971) 96.
[9] M. Yudasaka, R. Kikuchi, T. Matsui, H. Kamo, Y. Ohki and S. Yoshimura, *Appl. Phys. Lett., 64* (1994) 842.
[10] A.R. Ubbelohde, *Proc. R. Soc. London, Ser. A, 321* (1972) 445.
[11] G.M.T. Foley, C. Zeller, E.R. Falardean and F.L. Vogel, *Solid State Commun., 24* (1977) 371.
[12] C. Kittel, *Introduction to Solid State Physics*, Wiley, New York, 1986.